Bioorganic Chemistry 87 (2019) 169–180

Contents lists available at ScienceDirect

Bioorganic Chemistry

journal homepage: www.elsevier.com/locate/bioorg

Evaluation of guanylhydrazone derivatives as inhibitors of *Candida rugosa* digestive lipase: Biological, biophysical, theoretical studies and biotechnological application

Camilla C. Santana[a], Edeíldo F. Silva-Júnior[a,b], João César N. Santos[b], Érica E. da S. Rodrigues[a], Isabella M. da Silva[b], João X. Araújo-Júnior[a,b], Ticiano G. do Nascimento[a], Leandro A. Oliveira Barbosa[c], Camila B. Dornelas[a], Isis M. Figueiredo[b], Josué Carinhanha C. Santos[b,*], Luciano Aparecido M. Grillo[a,*]

[a] Nursing and Pharmacy School, Federal University of Alagoas, Maceió, Brazil
[b] Chemistry and Biotechnology Institute, Federal University of Alagoas, Maceió, Alagoas, Brazil
[c] Laboratory of Cell Biochemistry, Federal University of São João del Rei, Dona Lindú Centro-Oeste Campus, Divinópolis, Minas Gerais, Brazil

ARTICLE INFO

Keywords:
Digestive lipase inhibitors
Guanylhydrazone compounds
Fluorescence interaction studies
Rhynchophorus palmarum control

ABSTRACT

This work aimed to evaluate the inhibition of *Candida rugosa* lipase by five guanylhydrazone derivatives through biological, biophysical and theoretical studies simulating physiologic conditions. The compound **LQM11** (IC_{50} = 14.70 μM) presented the highest inhibition against the enzyme. Therefore, for a better understanding of the interaction process, spectroscopic and theoretical studies were performed. Fluorescence and UV–vis assays indicate a static quenching mechanism with non-fluorescent supramolecular complex formation and changing the native protein structure. The binding process was spontaneous ($\Delta G < 0$) and electrostatic forces ($\Delta H < 0$ and $\Delta S > 0$) played a preferential role in stabilizing the complex ligand-lipase. The compounds were classified as non-competitive inhibitors using orlistat as a reference in competition studies. Based on the ^{1}H NMR assays it was possible to propose the sites of ligand (epitope) that bind preferentially to the enzyme and the theoretical studies were consistent with the experimental results. Finally, **LQM11** was efficient as a lipase inhibitor of the crude intestinal extract of larvae of *Rhynchophorus palmarum*, an important agricultural plague, showing potential for control of this pest. Within this context, the real potential of this biotechnological application deserves further studies.

1. Introduction

Guanylhydrazone derivatives represent a class of compounds showing critical pharmacological properties. Some studies have shown antiproliferative activity in human cancer cell lines, antibacterial, anti-Trypanosoma and antifungal activities and also anti-glycating activity [1]. The aminoguanidine presents a versatile moiety with hydrogen bond acceptor and donor properties as well as being able to establish electrostatic interactions [1–5]. Noteworthy, there are many compounds that contain the hydrazone moiety in their structures with a sizeable biological profile, which, favors the use of these upon adipose-triglyceride lipases (ATGL), avoiding the increase of the plasma fatty acid (FA) levels [6].

In the last decades, several evidences have suggested that FA metabolism is closely related to the development of metabolic disorders. The increase of FA in the circulation, as verified in obesity, should be caused by FA overload of non-adipose tissues, resulting in triglyceride (TG) accumulation, which is related to impaired metabolic function of these tissues, insulin resistance, and inflammation [7,8]. In general, plasma levels of FA are determined by the action of lipases that catalyze the degradation of TG reserves in adipose tissue. Based on this, the decreasing of these levels is an exciting strategy to counteract the development of metabolic disease.

The *Candida rugosa* lipase (CRL) is an enzyme that consists of 535 amino acids in an alpha-beta hydrolase fold. Features of this protein include a hydrophobic core, a variety of *β*-sheet and helix secondary structure, and a lid formed by an amphipathic *α*-helix which covers the active site when closed and can spontaneously open to expose the active catalytic triad (Ser209-Glu341-His449) to the solvent [9,10]. However, the lid-opening event is thought to occur in the presence of phase

* Corresponding authors.
E-mail addresses: josue@iqb.ufal.br (J.C.C. Santos), luciano.grillo@esenfar.ufal.br (L.A.M. Grillo).

https://doi.org/10.1016/j.bioorg.2019.03.030
Received 1 August 2018; Received in revised form 3 March 2019; Accepted 14 March 2019
Available online 15 March 2019
0045-2068/

boundaries and hydrophobic environments [6]. Moreover, there is an oxyanion formed by Gly124 and Ala210. The formation of the oxyanion hole does not depend on the repositioning of amino acid residues following the opening of the lid [9]. The mechanism of the hydrolysis consists of several steps that remains to be fully elucidated, but a suggested pathway has been extrapolated based on similar mechanism to serine proteases; where the final step involves the release of a carboxylic acid [11–14].

In this context, CRL is an essential industrial enzyme with important, biotechnological applications, such as the production of FA and the synthesis of several esters [15,16]. Furthermore, it is applying as a biocatalyst to pharmaceuticals, cosmetics, textiles, and food industries [17,18]. Therefore, this enzyme was selected as the model for the inhibition studies.

The *Rhynchophorus palmarum* L. (Coleoptera: Curculionidae) feeds on the plant species of 12 different families and has been reported as one of the most important pests in commercial palm plantations [19]. Recently, lipase inhibition assays on the crude extract of the intestine of *Rhynchophorus palmarum* larvae indicates a new possibility for the control of this plague [20], which has not yet been explored.

This work aimed to evaluate the inhibition of CRL activity by guanylhydrazone derivatives through biological, biophysical and theoretical studies. From the guanylhydrazone derivatives, CRL activity inhibition assays were performed, and the compounds with higher and lower inhibitory effects were then selected for comparative analysis. Spectroscopic studies and a computer model were used to predict the behavior, thermodynamic parameters and types of interactions, using molecular dynamics and docking, and evidencing the properties of the interfacial activation, concerning the lipolytic activity decrease. Finally, the guanylhydrazone derivatives were assessed in the lipase inhibition assays on the crude extract of the intestine of *Rhynchophorus palmarum* larvae aiming a biotechnological application.

2. Experimental

2.1. Reagents and solutions

The enzyme used in the inhibition assays and interaction studies was a commercial lipase from *Candida rugosa* type VII (1135 units mg^{-1}). This enzyme, 2,3-dimercapto-1-propanol tributyrate (DMPTB), 5,5′-dithiobis(2-nitrobenzoic acid), Triton X-100, Tris-HCl, orlistat, 8-anilinonaphthalene-1-sulfonic acid (ANS), hydrochloric acid 37%, deuterium oxide (D_2O) and 4-methyl-umbelliferyl butyrate were obtained from Sigma-Aldrich® (St. Louis, EUA). Other reagents and solvents employed in the assays were of analytical grade with purity above 98% (DMSO, ethanol, EDTA, sodium trimethylsilyl propionate (TMSP), sucrose, NaH_2PO_4, Na_2HPO_4 and NaOH). Stock (1 mM) and work solutions (0.1 mM) of guanylhydrazones derivatives synthesized (according to item 2.2) and CRL (2 mg mL^{-1}) were prepared in 50 mM Tris-HCl buffer (pH 8.0 ± 0.1). Ultrapure water (18.2 MΩ cm^{-1}) was used in all the experiments to prepare the solutions (Millipore, USA). The variations in the concentrations of enzyme and guanylhydrazones derivatives employed in the different experiments are related to the sensitivity and specificities of each technique or method applied.

2.2. Guanylhydrazone derivatives

Guanylhydrazones (LQM, Fig. 1) were prepared by the reaction of aminoguanidine hydrochloride (1 eq.) and 4-chlorobenzaldehyde (**LQM02**), 4-cyanobenzaldehyde (**LQM03**), 4-hydroxyl-3,5-*tert*-butyl benzaldehyde (**LQM10**), 4-formyl benzoic acid (**LQM11**), or methyl 4-formyl benzoate (**LQM16**) (1.25 eq.). The reactants were added in 6 mL of methanol under reflux and stirred during the overnight. Additionally, all reactions were monitored by thin layer chromatography. Subsequently, the crude solutions were dried under reduced pressure. Finally, the solid materials were triturated, washed, and filtrated with cold ethyl acetate, leading to the substances as pure powders. All proceeds were performed as described by França et al. [21].

2.3. Lipase inhibitory activity assay in vitro

Lipase activity screening was assayed as described by Choi et al. [22]. A standard mixture was prepared using the final concentration of 0.2 mM of 2,3-dimercapto-1-propanol tributyrate (DMPTB), 0.8 mM of 5,5′-dithiobis(2-nitrobenzoic acid) (DTNB), 1 mM EDTA, 0.005% (m/v) of Triton X-100, 2 U of the enzyme (1.8 µL of 1 mg mL^{-1} solution) in 50 mM of Tris-HCl buffer (pH 8.0 ± 0.1), incubated at 37 °C. A control in the absence of DMPTB was employed. Inhibition of CRL activity by guanylhydrazone derivatives (200 µM) was evaluated by pre-incubation (10 min). After this, the absorbance at 405 nm was measured. CRL and crude extract from the anterior and posterior gut of *Rhynchophorus palmarum* larvae were used as the source of enzymes for the inhibition assays. The assays for inhibition concentration (IC_{50}) calculations were performed using the fluorogenic substrate 4-methyl-umbelliferyl butyrate (MUF-butyrate) based on Diaz et al. [23]. The lipolytic activity was evaluated according to the intensity of fluorescence emission due to the hydrolysis of the MUF-butyrate substrate and release of the MUF (fluorescent probe) in the reaction medium. The IC_{50} value has determined employing the statistical method of the sigmoidal dose-response curve.

2.4. Biotechnological application: insects and enzyme sources

The larvae (third instar) of *Rhynchophorum palmarum* employed in this study were fed exclusively with living vegetative tissue and taken from a colony maintained at 28 °C with 80% relative humidity. The foregut and hindgut of *Rhynchophorum palmarum* larvae were dissected. the luminal content was removed and the tissues were homogenized in a cold buffer (20 mM Tris-HCl at pH 8.0 containing 0.25 M sucrose) and used as sources of enzyme [19]. Protein concentrations were determined as described by Bradford using bovine serum albumin as standard [24].

2.5. Biophysical studies exploring spectroscopic techniques

The molecular fluorescence spectra in the steady-state mode were obtained using a spectrofluorophotometer model RF-5301PC (Shimadzu, Japan) with a xenon lamp (150 W) as the radiation source. The measurements were made in a quartz cuvette with an optical path of 1.0 cm. The excitation and emission slits were 5 and 10 nm, respectively. In the spectrofluorometric titrations of CRL (0.1 mg mL^{-1}, $\lambda_{ex}/\lambda_{em}$ = 280/343 nm), the concentration of **LQM11** or **LQM16** varied from 0 to 100 µM. The spectrofluorometric titrations were performed at different temperatures (22, 30 and 38 °C).

For the 3D-fluorescence experiments, CRL solutions (0.1 mg mL^{-1}) in the absence and presence of **LQM11** or **LQM16** (60 µM) were excited in the 220–350 nm range with emission spectra recorded from 250 to 650 nm.

Synchronous fluorescence studies were applied to monitor the tryptophan (Δλ = 60 nm) and tyrosine (Δλ = 15 nm) residues separately, as well as the evaluation of the microenvironment polarity of these amino acids in the enzyme [25]. Finally, orlistat (10 and 30 µM) was used as a competitive lipase inhibitor in the competition assay with guanylhydrazone derivatives by the active site of the enzyme.

The UV–vis experiments were performed employing spectrophotometer AXJ-6100PC (Micronal, Brazil) of double beam equipped with a quartz cuvettes pair having 1.0 cm of the optical path. The spectra of CRL (0.2 mg mL^{-1}), guanylhydrazone derivatives (10 µM) and the respective mixture (CRL + **LQM11** or **LQM16**) were obtained in the absorbance module at 30 °C.

The interaction between CRL and guanylhydrazone derivatives by ^{1}H NMR was evaluated based on **LQM11** or **LQM16** (1 mM) spectra

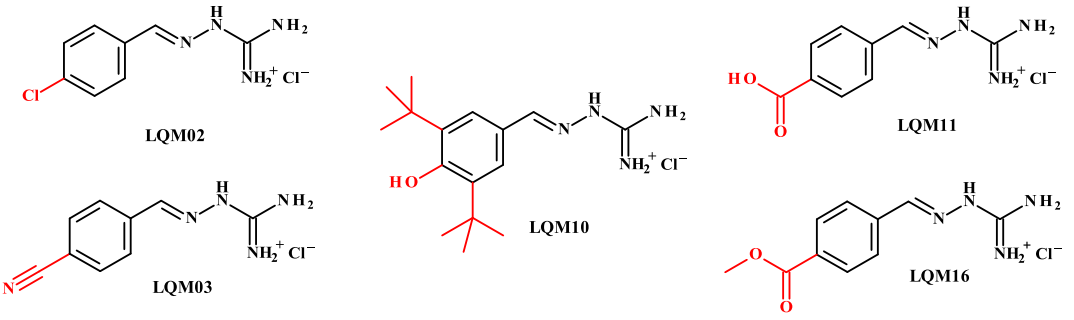

Fig. 1. Chemical structure of LQM guanylhydrazone derivatives evaluated as CRL inhibitor.

profile in the absence and presence of 0.4 mg mL^{-1} of the enzyme. The spectra were obtained on a Bruker 400 MHz spectrometer (B_0 = 9.4 T), using an indirect detection probe of 5 nm at 22 °C. The solutions were prepared in 10 mM phosphate buffer (pH 8.0) using H_2O/D_2O (1:10) containing 40 μM of sodium trimethylsilyl propionate (TMSP) [26,27]. In the experiments containing the mixture CRL and guanylhydrazone derivatives the resolution, peaks multiplicity, and variation of the chemical shift (δ) were used as an evaluation parameter.

2.6. Theoretical studies of CRL with guanylhydrazone derivatives (*LQM11* and *LQM16*)

2.6.1. Molecular dynamics simulations

The X-ray crystal structure (2.1 Å resolution) of the Lipase from *Candida rugosa* (PDB entry: 1TRH) was selected for carrying out the molecular dynamics (MD) simulations. All hydrogen atoms were added using the AutoDock Tools® version 1.5.4 (http://mgltools.scripps.edu/downloads/previous-releases/mgltools-1-5.4/mgltools-1-5.4) [28]. Moreover, the pK_a values of the macromolecule were estimated applying the empirical PROPKA® version 3.1 at pH 7.4 (physiological conditions) [29–31]. Gromacs® 2016 software (http://www.gromacs.org/) was used to perform the MD simulations. In total, fourteen sodium counterions (Na^+) were added into the system to obtain electroneutrality, and the full system was placed in an orthorhombic box of water molecules (1000 $Å^3$). The CRL structure and water molecules were minimized by OPLS force field, implemented in the Gromacs® 2016 program. In a sense, the Simple Point Charge (SPC) 2016 model was used to describe the water solvation model [13]. The complete system was described as a total of 46,210 atoms, and it was relaxed for 20 ns at 300 K. Finally, to validate the CRL structure generated by MD the Ramachandran plots were obtained using Rampage® server (http://mordred.bioc.cam.ac.uk/~rapper/rampage.php) developed by Crystallography and Bioinformatics Group from the University of Cambridge [32].

2.6.2. Molecular docking

In the studies, by molecular docking, the ligand structures were drawn in .smiles* format, and they were converted into three-dimensional .mol2* files using Corina® (Molecular Networks, http://www.molecular-networks.com/) [33]. Austin Model (AM1) was employed as a method for energy minimization by ArgusLab® version 4.0.1 (http://www.arguslab.com/arguslab.com/ArgusLab.html). All final structures were converted in .pdbqt* files by AutoDock Tools® version 1.5.6. The ligand structures were considered into pH 7.4 (at physiological conditions). Finally, the protonation states were generated using the Fixpka from QUACPAC® version 15.0 program (http://www.eyesopen.com/news/quacpac-v150-released). Furthermore, ions and water molecules from the more stable CRL generated by MD simulations were removed, using the graphical interface of AutoDock Tools v. 1.5.6 [33]. Based on the possibility that there is an allosteric binding site, the blind-docking method was employed as a more convenient docking protocol. In sense, a grid box centered on *x*: −0.06; *y*: 0.096; and *z*: 0.289 Å was applied. This grid was used to evaluate the steric boundary of the CRL and van der Waals and/or hydrogen bond interactions between the ligands and the binding site [34]. Partial atomic charges were added by using the Kollman mathematical method, and all atoms were assigned as AD4 type. Finally, the molecule was converted to .pdbqt* extension [35,36].

2.6.3. Gibbs free energies of binding (ΔG) determination by density functional theory

Recently, several studies using broadly employed docking programs concluded that no docking program is capable of predicting accurate Gibbs free energy of binding (ΔG) [37–40]. On the other hand, the ΔG between a ligand and macromolecular target can be accurately obtained from the application of rigorous chemical calculations, based on quantum chemistry [41,42]. The Density Functional Theory (DFT) calculations were performed using the M06/6-31G(d) level of theory from the Spartan® version 14.0 program. This level of theory was applied to provide the corrected values of ΔG from the ligands-CRL complex formation. The M06 method applies the global hybrid functional, which is the top performer within the six functionals of the leading group, thermochemistry, kinetics and non-covalent interactions [43–45]. In a sense, the correct structures of the ligands and their active sites into CRL structure were required, whose they were extracted from the molecular docking studies.

The binding energy values were obtained applying the Eq. (1), where the ΔG was calculated as the difference between the complex energy ($E_{complex}$) and the sum of the CRL enzyme (E_{enzyme}) and ligand (E_{ligand}) energies considered separately:

$$\Delta G = [E_{complex} - (E_{enzyme} + E_{ligand})] \quad (1)$$

In these calculations, the electrostatic and steric effects of the protein environment surrounding the active site were ignored entirely. Finally, all these procedures were performed as described by Silva-Júnior et al. [42].

3. Results and discussion

3.1. Biological studies: inhibition of the lipase activity and IC_{50} determination in vitro

The inhibition assays using a commercial *C. rugosa* lipase (CRL) showed a significant inhibition only with the guanylhydrazone derivatives **LQM02** and **LQM11**, with a lipase activity reduction of 23 and 47%, respectively. For the other derivatives insignificant percentages of inhibition were observed: **LQM03** (0.0%), **LQM010** (5.43%) and **LQM016** (7.31%) (Fig. 2A).

To evaluate the inhibition profile and predict the possible interactions between guanylhydrazone derivatives and enzyme, **LQM11** and **LQM16** compounds were selected (based on higher and lower inhibitory effect, respectively) to proceed in more specific interaction studies. The major structural difference between the guanylhydrazone derivatives is the carboxylic acid function (completely dissociated at pH 8.0) in **LQM11**, while **LQM16** presents the corresponding methyl ester.

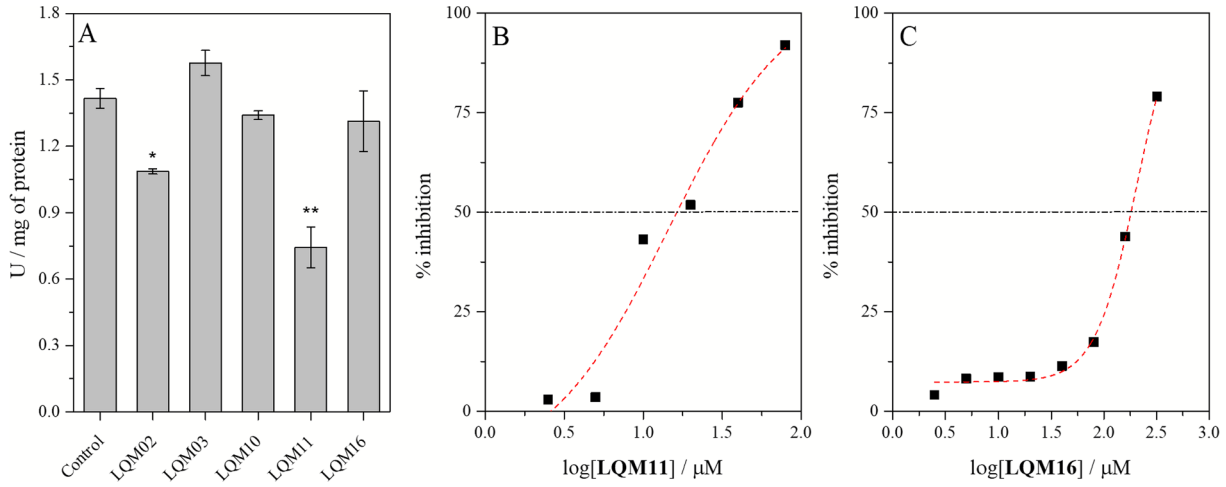

Fig. 2. (A) Effect of guanylhydrazone derivatives on the activity of CRL. For the screening assay, enzyme activity was assessed containing 200 μM of guanylhydrazones derivatives at pH 8.0. (B) LQM11 and (C) LQM16 dose–response curve profile for inhibition concentration (IC_{50}) determination. The error bars represent the SD for the three determinations (ANOVA/Bonferroni test: $^{*}p < 0.05$; $^{**}p < 0.0001$).

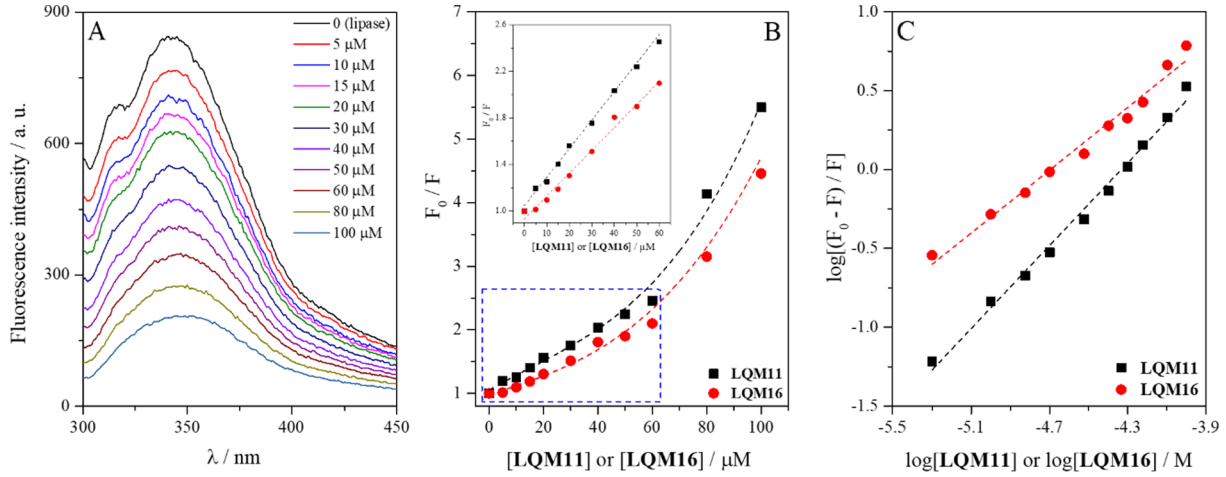

Fig. 3. (A) Lipase from *Candida rugosa* (0.1 mg mL^{-1}) emission spectral profile at different concentrations of LQM11 from 0 to 100 μM in pH 8.0 and 30 °C. (B) Stern-Volmer quenching plot. The inset in (B) corresponds to a linear range in the Stern-Volmer plot. (C) Double logarithmic curve to the binding constant calculation.

The small structural variation in the compounds (methyl group) led to the inhibition of selectivity in CRL activity (Fig. 2A).

The methylation effect on physical, chemical and biological properties of different compounds, is widely discussed and supported by Barreiro et al. [46]. Thus, a functional change of this nature may actually lead to effective variations in the inhibitory profile of the evaluated compounds.

Therefore, the half maximal inhibitory concentration (IC_{50}) was calculated for both guanylhydrazone derivatives. The compound with higher inhibitor effect (**LQM 11**) showed IC_{50} of 14.70 ± 0.61 μM (Fig. 2B), while the compound with lower inhibitor effect (**LQM16**), showed IC_{50} of 171.8 ± 1.6 μM (Fig. 2C), consequently, the **LQM11** derivative was approximately 12 times more active than its analogous.

Finally, the guanylhydrazone derivative **LQM11** presents IC_{50} value comparable to other lipase inhibitors (in vitro assays) reported in the literature for synthetic and natural compounds against different enzymes models (Table S1, supplementary material). Surprisingly, the compound **LQM11** was more active against the CRL when compared to the orlistat (IC_{50} = 137.2 μM at pH 7) [47].

3.2. Evaluation of interaction process by biophysical studies

The biophysical studies based on different spectroscopic techniques were applied to obtain a mutual understanding of enzymatic inhibition process of CRL by guanylhydrazone derivatives **LQM11** and **LQM16**.

3.2.1. Binding and thermodynamics parameters exploring fluorescence spectroscopy

Proteins generally have three intrinsic fluorophores: tryptophan (Trp), tyrosine (Tyr), and phenylalanine (Phe) residues. The Phe residue has low fluorescence quantum yield, while Tyr residue fluorescence is almost entirely quenched by the carboxyl group, disulfide bonds or Trp residue. Lipase from *C. rugosa* contains five Trp residues at locations 119, 161, 188, 221 and 489 and twenty Tyr residues [48]. The CRL intrinsic fluorescence is contributed mainly by Trp residues, which can be used as intrinsic fluorophores to provide information on the enzyme-ligand interaction and ligand-induced conformational change around the binding site [26]. Thus, the binding and thermodynamic parameters of CRL and the guanylhydrazone derivatives **LQM11** and **LQM16**, with higher and lower inhibitory effect, respectively, were established exploring fluorescence spectroscopy.

The evaluation of interaction among guanylhydrazones derivatives (**LQM11** and **LQM16**) and CRL was explored by spectrofluorometric titration based on protein intrinsic fluorescence. The fluorescence spectra profile of CRL titrated with the ligand **LQM11** is shown in Fig. 3A. A similar spectral profile was obtained to CRL when titrated

with **LQM16** in the same experimental conditions.

The CRL presented an intense and broad band, centered at 343 nm when excited at 280 nm and the ligands addition carried out the decrease in fluorescence intensity, besides emission band shift from 343 to 345 nm. The redshift caused by ligands interaction with CRL lead to exposure of the Trp to a more polar microenvironment, indicating a change in the conformational of the native enzyme [49]. Thus, to examine the mechanism of interaction between **LQM11** and **LQM16** with CRL the Stern-Volmer equation was applied:

$$\frac{F_0}{F} = 1 + K_q \tau_0 [Q] \quad or \quad \frac{F_0}{F} = 1 + K_{SV}[Q] \tag{2}$$

F_0 and F are the fluorescence intensities in the absence and the presence of the ligand, respectively; K_q is the bimolecular diffusion quenching rate constant, τ_0 is the average lifetime (10^{-8} s), [Q] is the ligand concentration (quencher), and K_{SV} is the Stern-Volmer quenching constant [27]. The binding constant was calculated according to Eq. (3):

$$\log\left[\frac{(F_0 - F)}{F}\right] = \log K_b + n\log[Q] \tag{3}$$

K_b is the binding constant and *n* is the number of binding sites. The Fig. 3B-C shows linearization of the Eqs. (2) and (3), respectively, to calculate the binding parameters (K_{SV}, K_b, and *n*). The temperature effect on the interaction process between guanylhydrazones derivatives (**LQM11** and **LQM16**) and CRL was further investigated and the results summarized in Table 1.

The exponential profile of K_{SV} plot (Fig. 3B) indicates that all Trp residues are accessible to the quencher or, only one of Trp residues is responsible for fluorescence emission [50]. The concentration linear range obtained employing guanylhydrazone derivatives from 5.0 to 60 μM was employed to calculate K_{SV} values (Table 1) and determine the quenching mechanism. The K_{SV} values decreased upon an increment of temperature from 22 to 38 °C, indicating the occurrence of static quenching, due to higher temperatures that affect the enzyme-ligand complex stability [51]. According to Das et al. [52], when the K_q is less than 2.0×10^{10} M^{-1} s^{-1} occurs a dynamic quenching, while higher K_q values are an indication of static quenching mechanism. The K_q values obtained in this study (Table 1) varied from 1.87 to 2.55×10^{12} M^{-1} s^{-1}, confirming that the interaction process occurs through the static quenching.

The ligand affinity with CRL is a relevant parameter for the enzyme-ligand interaction study and thereby helps to explain the lipase inhibition profile. The K_b values for the guanylhydrazone derivatives and CRL complexes interaction ranged from 4.48 to 5.17×10^5 M^{-1} for **LQM11** and 0.41 to 0.54×10^5 M^{-1} for **LQM16** based on temperature variation (Table 1), and the *n* was close to unity indicating that there is a single site of binding of the ligands with the enzyme. Therefore, the compound **LQM11** presented more affinity towards CRL, since the K_b values were ~11-folder higher than that of **LQM16** (at 38 °C), corroborating with the biological activity assay, being obtained an IC_{50} value for **LQM11** ~12-folder higher than that of **LQM16**.

Binding sites number (*n*) were calculated and varying from 1.05 to 1.27, indicating the interactions among **LQM11** and **LQM16** with CRL occur in the ratio 1:1. Additionally, the guanylhydrazone derivatives assessed showed binding constant values comparable to other compounds interacting with different lipases models (Table S2).

The thermodynamic parameters (ΔH and ΔS) were calculated according to the linearization of the Van't Hoff equation (Fig. S1, supplementary material) whereas the heat of reaction did not change with temperature [53]:

$$\ln K_b = -\frac{\Delta H}{R}\left[\frac{1}{T}\right] + \frac{\Delta S}{R} \tag{4}$$

K_b is the binding constant, T is the temperature in Kelvin (K), and R is the universal gas constant (Eq. (4)). The Gibbs free energy (ΔG) value was obtained using the following equation:

$$\Delta G = \Delta H - T\Delta S \tag{5}$$

The calculated thermodynamic parameters are presented in Table 1. According to Ross and Subramanian [54], when $\Delta H < 0$ and $\Delta S > 0$ the interaction between **LQM11** and **LQM16** with CRL is preferably governed by electrostatic forces. This fact can be justified by the chemical structure of the compounds, since protonation of the positively charged amine groups (in both compounds) and dissociation of the carboxylic acid group with a negative charge (in **LQM11**) are expected. Besides, it was evident that the interaction of **LQM11** was more associated to enthalpic factors, whereas that of **LQM16,** to entropic factors. Finally, all values of ΔG were negative indicating the spontaneity of the interaction.

3.2.2. UV–vis evaluation of interaction process

The UV–vis spectroscopy was used to assess the formation of the guanylhydrazone derivatives and CRL complexes based on monitoring of the structural changes in the protein, besides confirming the quenching mechanism related with the fluorescence suppression process [55].

The free CRL presented maximum absorption at 277 nm associated to aromatic residues of Trp, Tyr and Phe absorption due to the transitions $\pi \rightarrow \pi^*$ [50], while the λ_{max} for **LQM11** and **LQM16** were 313 and 317 nm, respectively, because the transitions $\pi \rightarrow \pi^*$ and $n \rightarrow \pi^*$ (Fig. S2). Once **LQM11** was added to the CRL solution, it was verified a hyperchromic effect followed by a 29 nm bathochromic shift, indicating an interaction between enzyme and ligand with the supramolecular complex formation. The spectrum acquired from subtraction of the complex spectra by the free ligand (**LQM11**) resulted in a non-overlapping spectrum to the free CRL spectrum (Fig. S2A), proving that there was no additive effect of Beeŕs law (Table S3) and confirming the enzyme and **LQM11** complex formation. Similar results were obtained for guanylhydrazone derivative **LQM16** (Fig. S2B). Since that supramolecular complex formation shown by UV–vis is related with changes in the ground state of evaluated compounds (**LQM11** and **LQM16**) and

Table 1
Binding and thermodynamic parameters of the interaction process of **LQM11** and **LQM16** with CRL.

Compound	T (°C)	Quenching parameters			Binding parameters			Thermodynamic parameters**		
		K_{SV} (10^4 M^{-1})	*r**	K_q (10^{12} M^{-1} s^{-1})	K_b (10^5 M^{-1})	*n*	*r**	ΔH (kJ mol^{-1})	ΔS (J mol^{-1} K^{-1})	ΔG (kJ mol^{-1})
LQM11	22	2.55 ± 0.08	0.9976	2.55	5.17 ± 0.24	1.27 ± 0.07	0.9942	− 29.67	+ 2.93	− 28.84
	30	2.46 ± 0.09	0.9963	2.46	4.92 ± 0.19	1.29 ± 0.04	0.9972			− 28.81
	38	2.38 ± 0.01	0.9959	2.38	4.48 ± 0.11	1.17 ± 0.06	0.9964			− 28.79
LQM16	22	2.05 ± 0.05	0.9974	2.05	0.54 ± 0.03	1.09 ± 0.05	0.9962	− 13.46	+ 25.86	−5.83
	30	1.98 ± 0.03	0.9992	1.98	0.47 ± 0.01	1.05 ± 0.03	0.9951			−5.62
	38	1.87 ± 0.02	0.9978	1.87	0.41 ± 0.02	1.07 ± 0.04	0.9948			−5.42

* *r* represents the linear correlation coefficient (Pearson coefficient).
** ΔH = enthalpy change, ΔS = entropy change and ΔG = Gibbs free energy.

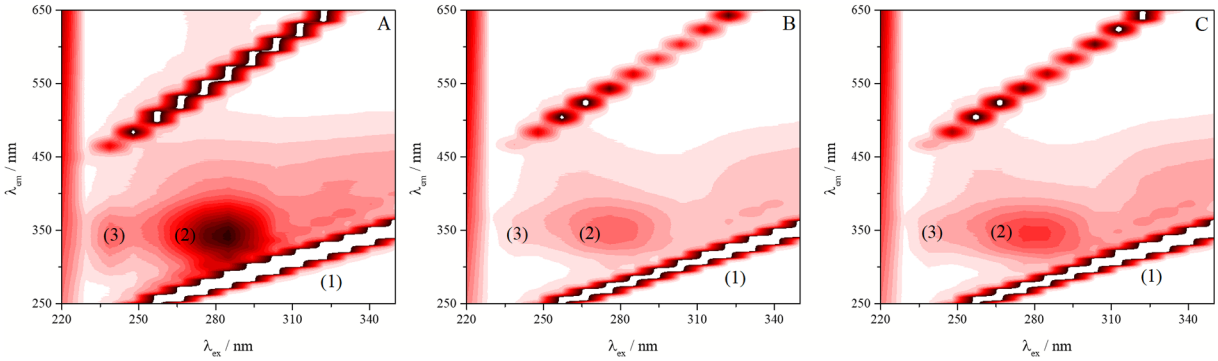

Fig. 4. Tridimensional fluorescence spectra of (A) CRL (B) CRL-LQM11 and (C) CRL-LQM16 complex. Enzyme and ligands at 0.1 mg mL^{-1} and 60 μM, respectively, all systems at pH 8.0 and 30 °C.

CRL in the interaction process [51,52], the static quenching mechanism previously reported by molecular fluorescence results is confirmed.

3.2.3. Evaluation of conformational changes in the structure of CRL

3.2.3.1. Three-dimensional fluorescence spectroscopy. The three-dimensional (3D) fluorescence spectroscopy allows a study of the conformational changes in the secondary structure of the proteins [25–27]. The 3D fluorescence spectra for CRL and several complexes with **LQM11** and **LQM16** are presented in Fig. 4.

The 3D fluorescence spectrum of free CRL (Fig. 4A) and the complexes of **LQM11** and **LMQ16** with the enzyme (Fig. 4B and C) presented three peaks (1, 2 and 3). The peak 1 corresponds to Rayleigh scattering, which is characterized by radiation re-emission ($\lambda_{ex} = \lambda_{em}$) by solvent (water) of the medium; thereby a small fraction of the absorbed radiation is scattered in all directions at the same wavelength. The peak 2 is related to the emission of Trp and Tyr residues, and peak 3 to the emission of the polypeptide backbone of the CRL [56]. After guanylhydrazone derivatives addition, the fluorescence intensity of the peaks 2 and 3 were reduced 67 and 64% for **LQM11** and 59 and 41% for **LQM16**, respectively (Table 2).

The reduction in the fluorescence signal of the peak 2 indicates changing in the Trp and Tyr microenvironment, while for peak 3, indicates a modification in the native protein structure. The most significant variations in polypeptide protein chain and enzyme folding were verified for the CRL-**LQM11** complex. Thus, the ability of **LQM11** to change the original conformation of the CRF is probably one of the reasons of its efficiency as lipase inhibitor. Additionally, the change in the λ_{ex} or λ_{em} related to the fluorescence peaks (2 and 3) indicates that the native protein structure was altered. Similarly, it was verified by Stokes shift in each system in comparison with free CRL that **LQM11** presented the highest variation, corroborating the previous results.

3.2.3.2. Synchronous fluorescence. Based on synchronous fluorescence measures, it is possible to monitor the interaction process and changes in the microenvironment polarity of the Trp and Tyr residues, separately [57]. In this study, Stern-Volmer constant (K_{SV}) based on $\Delta\lambda$ = 15 nm (Tyr) and $\Delta\lambda$ = 60 nm (Trp) was the analytical parameter used to evaluate interaction between guanylhydrazones derivatives and CRL. Synchronous fluorescence spectra profile for CRL and **LQM11** system at pH 8.0 is shown in Fig. 5, and similar results were obtained for **LQM16**. The Table S4 presented binding parameters obtained for guanylhydrazones derivatives evaluated with CRL.

Considering the results obtained an emission maximum shift for both evaluated compounds was observed against the enzyme (Fig. 5 and Table S4). For the **LQM11** and **LQM16** the shifts were more pronounced for Tyr residues than Trp, probably is due to these residues, in the CRL structure, are more accessible to ligands in comparison to Trp. The real variation indicates an increase in polarity of the microenvironment, as well as negative variation is related to polarity reduction, and both processes allow describing changes in the original protein structure [58].

According to the K_{SV} values Tyr residues of CRL were systematically most affected when compared to Trp (Table S4) and had their microenvironment changed more significantly than Trp, in the interaction process. The results obtained by synchronous fluorescence were in agreement with those achieved by molecular docking (presented at the theoretical studies session).

3.2.4. Protein binding site evaluation

For evaluation of the preferential binding sites between the guanylhydrazone derivatives and the CRL, compounds with selectivity by some areas of the enzyme were used, thus acting as labeling probes. This strategy has been successfully used to evaluate the preferential binding site in enzymes (urease) [25], and carrier proteins (HSA and BSA) [27].

Orlistat is a compound that binds to the catalytic site of lipase being a competitive inhibitor [47]. To evaluate the site interaction in the CRL with guanylhydrazone derivatives (**LQM11** and **LQM16**) spectrofluorometric titration based on intrinsic protein fluorescence was performed in the presence and absence of the competitor (orlistat). The ratio between binding constants was used as the evaluation parameter, where K_b' is the constant in the presence of the orlistat (at two different

Table 2
Three-dimensional fluorescence spectrum parameters for the CRL and the complexes with **LQM11** and **LQM16**. Conditions: pH of 8.0 at 30 °C.

Peak	CRL			CRL + **LQM11**			CRL + **LQM16**		
	Position ($\lambda_{ex}/\lambda_{em}$)[a]	Stokes shift $\Delta\lambda$ (nm)[b]	Fluorescence intensity	Position ($\lambda_{ex}/\lambda_{em}$)[a]	Stokes shift $\Delta\lambda$ (nm)[b]	Fluorescence intensity	Position ($\lambda_{ex}/\lambda_{em}$)[a]	Stokes shift $\Delta\lambda$ (nm)[b]	Fluorescence intensity
(1) Rayleigh scattering	$\lambda_{ex} = \lambda_{em}$	0	> 1015	$\lambda_{ex} = \lambda_{em}$	0	> 1015	$\lambda_{ex} = \lambda_{em}$	0	> 1015
(2) Trp and Tyr	285/342	55	878 (100%)	276/350	74	292 (33%)	276/346	70	361 (41%)
(3) Polypeptide chain	238/339	101	295 (100%)	238/355	117	107 (36%)	248/352	104	173 (59%)

[a] Values in nm.
[b] $\Delta\lambda = \lambda_{em} - \lambda_{ex}$.

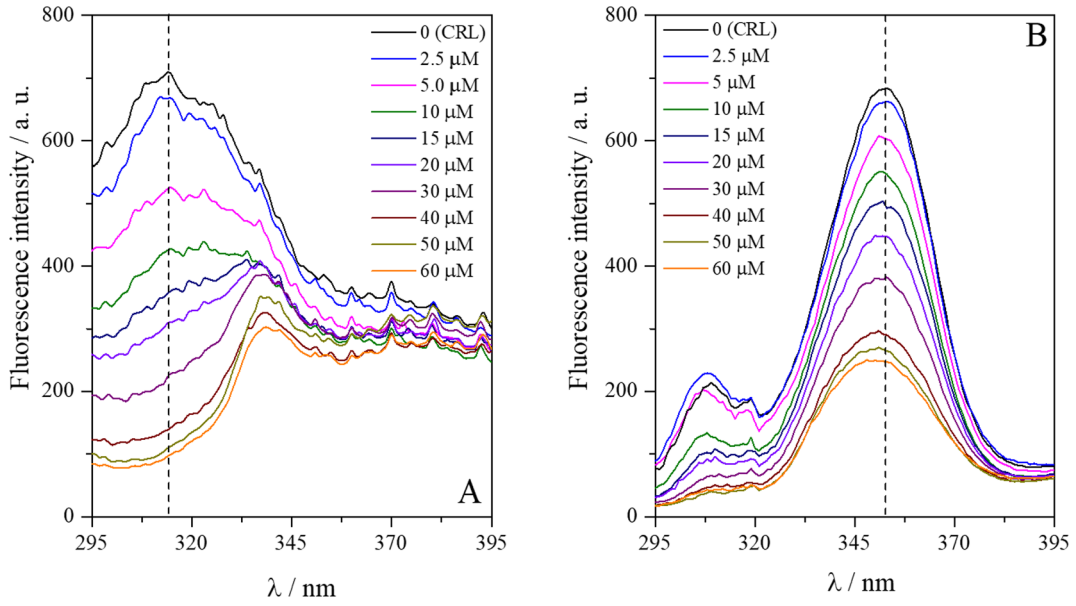

Fig. 5. Lipase from *Candida rugosa* (0.1 mg mL^{-1}) synchronous fluorescence spectra upon addition of increasing concentrations of LQM11 at different concentrations in pH 8.0 and 30 °C, monitoring (A) Δλ = 15 nm (Tyr) and (B) Δλ = 60 nm (Trp).

levels of concentration), and K_b in the absence of competitor. When the ratio $K_b'/K_b > 1$ indicate that complex between the evaluated guanylhydrazones and CRL is favored. On the other hand, for ratio $K_b'/K_b < 1$ occurs hindrance toward supramolecular complex formation due to competition among the **LQM11** or **LQM16** and orlistat, probably, by the same region, in this case, the catalytic site of the lipase.

The results showed that orlistat did not displace of **LQM11** or **LQM16** from the lipase binding site (Table 3), consequently, the guanylhydrazone derivatives and orlistat bind in different regions of the enzyme ($K_b'/K_b \approx 1$). Therefore, the central mechanism of action of the **LQM11** and **LQM16** is based on non-competitive inhibition, binding at an allosteric site of the CRL. The competitive assay with orlistat presented a good agreement with molecular docking results (presented at the theoretical studies session).

The 8-anilinonaphthalene-1-sulfonic acid (ANS) is a probe that selectively binds to hydrophobic regions of the proteins [59]. The ANS presents weak fluoresce in an aqueous medium, however, in the presence of the lipase, the probe binding in the protein hydrophobic sites and occur a significant increase in the fluorescence intensity (Fig. S3). When a ligand is capable of binding to the same ANS site, it is displaced, and the fluorescence intensity is reduced. In this study, none of the guanylhydrazone derivatives could replace the ANS (spectral overlap) of its hydrophobic site (Fig. S3A-B), which corroborates that main forces of complex formation are electrostatic based on thermodynamic parameters. Therefore, the binding site of LQM11 and LQM16 in the CRL should be a more polar region, compared at the ANS probe binding local.

3.2.5. Evaluation of the interaction process by ^{1}H NMR

In this study, it was possible to monitor changes in the ligands evaluated, while in the previous spectroscopic experiments, variations resulting mainly to the modifications in the protein structure were assessed [60]. Thus, the chemical shift (δ) was one of the parameters selected to monitor the effect of the interaction of **LQM11** and **LQM16** with the CRL by the nuclear magnetic resonance of hydrogen (^{1}H NMR). The ^{1}H NMR spectra of **LQM11** and **LQM16** in the absence and presence of CRL with all of the hydrogens assigned are shown in Fig. 6.

In the presence of an enzyme, the guanylhydrazone derivatives signals were observed to be enlarged. However, the chemical shifts varied only for the hydrogens Ha and Hc of **LQM11** (Table S5), due to intermolecular interaction between this compound and the enzyme. The variation in the chemical shifts (Δδ) for **LQM11** hydrogen atoms Ha and Hc in the absence and presence of CRL was ± 0.01 (Table S5). Thus, the region of the compound **LQM11** near the hydrogen atoms Ha and Hc (sites nearby the positive and negative charges of the compound), should be the epitope of the molecule, where the interaction process is most effective [26]. Finally, the ^{1}H NMR studies corroborate with the previous results, where the compound **LQM11** presented more significant interaction with the CRL in comparison to **LQM16**.

Table 3
CRL binding constants ratio of guanylhydrazone derivatives in the presence (K_b') and absence (K_b) of orlistat, a competitive lipase inhibitor. Conditions: pH of 8.0 at 30 °C.

Orlistat (μM)	Binding constant ratio (K_b'/K_b)	
	LQM11	**LQM16**
10	1.05	1.02
30	0.98	1.23

3.3. Evaluation of the interaction process by theoretical studies

3.3.1. Molecular dynamic

Initially, the generated 3D-structure of CRL enzyme by MD simulations was validated. The validation of the backbones and amino acid side chains for this model were performed by generating and analyzing the corresponding Ramachandran plots, which represent the distributions of the glycine and proline dihedral angles ϕ and ψ (Fig. S4).

The Ramachandran plotted was used to determine the validation of CRL enzyme generated by MD simulation. In a sense, it was verified that the 90% of the residues are in the most favored regions (dark blue) and 10%, in additional allowed regions (pale blue and orange). No amino acid residues were found in the disallowed region (white). The plots at the top- and bottom-left quadrants indicate that the model contains both -sheet and -helix structures (Fig. S4). Moreover, the plots at the top- and bottom-right quadrants represent the lid structure. Finally, these results prove that the model is highly plausible.

In general, CRL is active upon interfacial activation. Interfacial activation implies the opening of the lid, with the *cis-trans* isomerization of Pro92 and the shift of the lid almost 19.0 Å before the fatty acid can be adsorbed on the active site [61,62]. However, the only way that

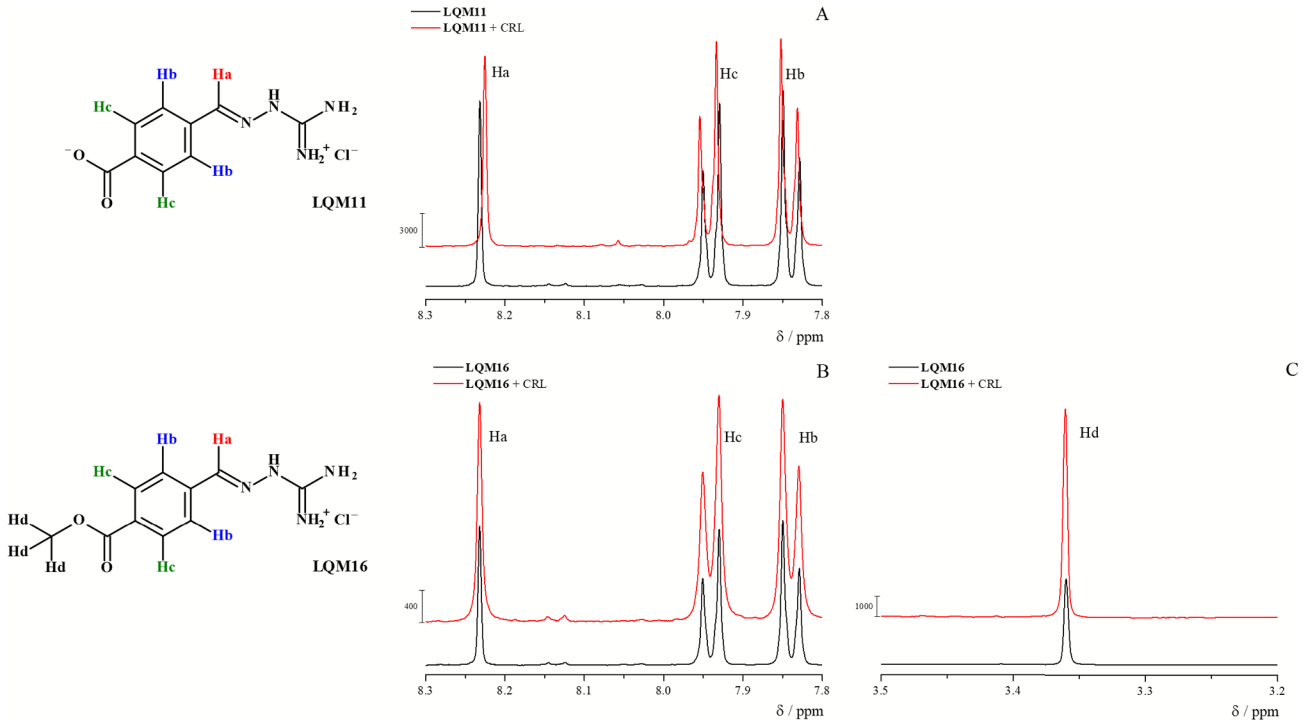

Fig. 6. ^{1}H NMR spectra (400 MHz) of (A) LQM11, (B) and (C) LQM16 in the absence and presence of CRL at pH 8.0 and 22 °C. Sodium trimethylsilylpropionate (TMSP) was employed as an internal reference standard.

proline in the CRL's lid can suffer isomerization is upon protonation and change of the amide N to a transition state with an ammonium character. Water or even buffer of pH 7.0 is not acidic enough to protonate N from proline [9]. Additionally, it is suggested that the reaction mechanism of CRL involves acylation and deacylation steps, similar to those of serine protease [11,63].

The CRL structure relaxes to a root-mean-square deviation (RMSD) of about 3.15 Å during the first six ns of MD simulation. The low RMSD value indicates that the enzyme exhibits a little conformational deviation from its starting structure. Additionally, it was observed that the CRL-**LQM11** complex stabilization occurs about 8.5 ns (Fig. 7A), and for the CRL-**LQM16** complex, about 15.8 ns (Fig. 7B).

The conformational stability of CRL-**LQM11** and CRL-**LQM16** complexes were investigated during the MD simulation. For this propose, the RMSD from the initial structure throughout the simulation was analyzed. In the Fig. 7A, it is possible to suggest that there is a transition state for CRL-**LQM11** complex formation, at five ns, whose it is stabilized after eight ns of dynamic simulation. At transition state, there is an RMSD gap of 1.45 Å which fall to 0.4 Å, after complex formation, suggesting a good affinity between them. For the CRL-**LQM16** RMSD (Fig. 7B), it is observed that the transitional state is not transparent, but the complex stabilization (RMSD gap value of 0.8 Å) occurs about of 15 ns, suggesting that the **LQM16** does not effectively interacts with CRL enzyme.

Interestingly, crystals of CRL enzyme can be found in a closed conformation, with the hydrophobic pocket and catalytic triad (Ser209, Glu341, and His449) obscured, such as 1TRH.pdb structure. Thus, the enzyme may be closed when soluble and may open to engaging a fat droplet at the catalytic site [61,64]. This fact was confirmed by a comparative study of the CRL crystal structure from PDB and CRL structure generated by MD simulation (Fig. 8A). In both cases, it was observed the closed conformation for the lid which became the catalytic triad inaccessible, by results observed by Burney et al. [6]. Furthermore, it was verified that the **LQM11** and **LQM16** preferentially interact with a completely different active site, mainly on the opposite side of the CRL enzyme (Fig. 8B).

Considering the closed lid conformation, the results corroborate the hypothesis that there is an allosteric site, due to the monitoring of distances and positions of the side chains of the catalytic residues Ser209, Glu341 and His449 not having showed any essential alterations in the structural organization of the catalytic triad, which suggests a non-competitive inhibition, a hypothesis corroborating the spectroscopic results.

3.3.2. Molecular docking

It is worth noticing that **LQM11** and **LQM16** interact with a different binding pocket, considering the catalytic triad. This fact contributes to suggest that there is an allosteric binding site involved in the activity of these compounds, supported by the experimental results. In Fig. 9 all interactions for these guanylhydrazone derivatives are shown.

Based on molecular docking it was verified that **LQM11** and **LQM16** compounds present van der Waals interactions with Pro43. Individually, the **LQM11** compound interacts with the Leu6, Gln187, and Asn192, hydrophobically. Also, it was also observed three H-bonds, such as COO^- group with $-C{=}NH_2^+$ at Trp188 (3.28 Å) and Pro27 (4.4 Å) residues; and $-C{=}NH_2^+$ group with COO^- at Tyr228 (2.83 Å) residue. These hydrogen interactions favor the complex stabilization and increase the affinity. In contrast, **LQM16** interacts with the Ala7, Trp188, and Tyr228 residues, hydrophobically. Moreover, there is an H-bond between $-C{=}NH_2^+$ and COO^- at Asn8 (3.24 Å) residue. Finally, it is possible to suggest that Pro43, Tyr188, and 228 amino acids should be considered as critical residues for allosteric modulation of CRL enzyme. However, Leu6, Pro27, Gln187, and Asn192 could contribute to the activity, as stabilizing residues.

3.3.3. Gibbs free energies of binding (ΔG) determination by density functional theory

Frequently, the algorithms used in molecular docking simulations are not able to predict accurate Gibbs free energies (ΔG) [62]. In a sense, quantum mechanical (QM) calculations can be applied as a safe method to predict ΔG values more reliable [42]. The binding pose for each ligand and their corresponding active sites were utilized as a

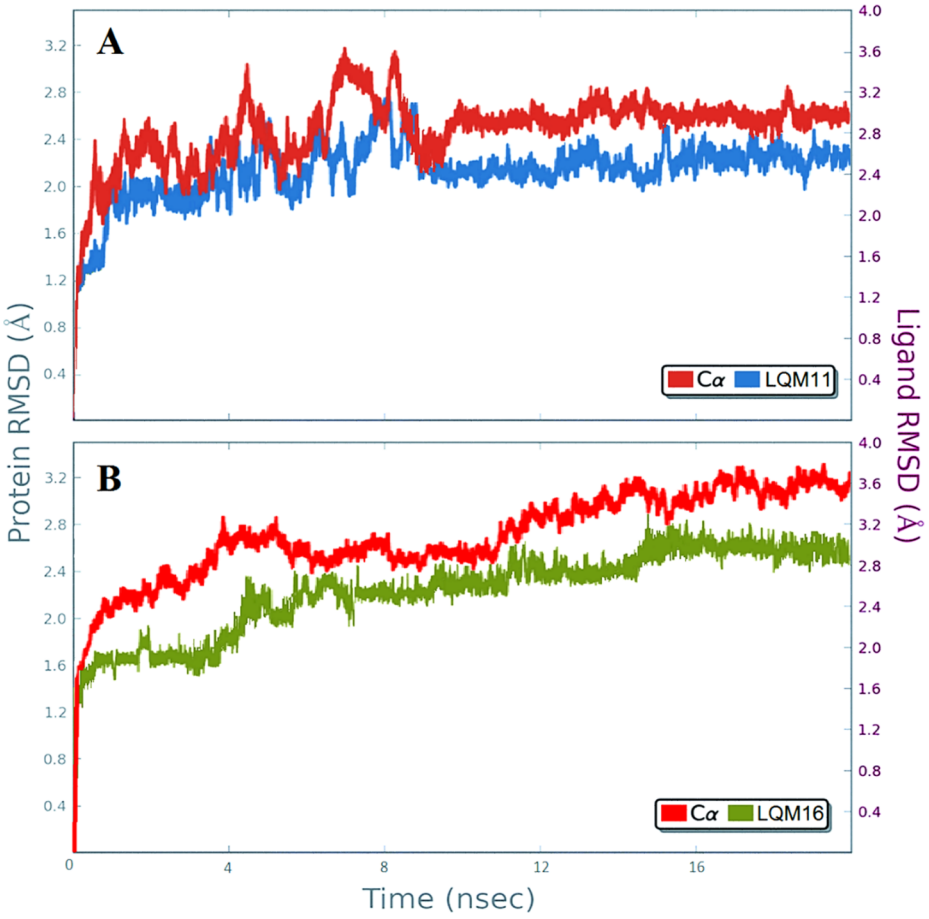

Fig. 7. Molecular dynamics trajectory plots correlating RMSD deviation from the initial CRL enzyme Cα-atoms and (A) LQM11 (blue) and (B) LQM16 (green) coordinates over a simulation time of 20 ns.

starting point, which was extracted from the molecular docking simulations. Based on this, DFT calculations using M06/6-31G(d) as the level of theory were applied to determine the corrected ΔG values from the CRL-guanylhydrazone derivatives complexes formation. Finally, all energetic values were calculated as described in the methods section. The results for this evaluation are shown in Table 4.

It is possible to observe that there is a relationship between the experimental and the predicted ΔG values by M06/6-31G(d). The **LQM11** presented a high affinity to the CRL enzyme, with a ΔG value of $-31.85\ \text{kcal mol}^{-1}$ (Table 4). In contrast, **LQM16** demonstrated a low affinity to the CRL, with a ΔG value of $-11.82\ \text{kcal mol}^{-1}$. Interestingly, some information can be derived from these QM calculations. Considering the structural similarity between both guanylhydrazone analogs, it is possible to verify the existence of significant energetic differences when all results are individually analyzed. In general, both compounds present similar E_{ligand} values, since they have

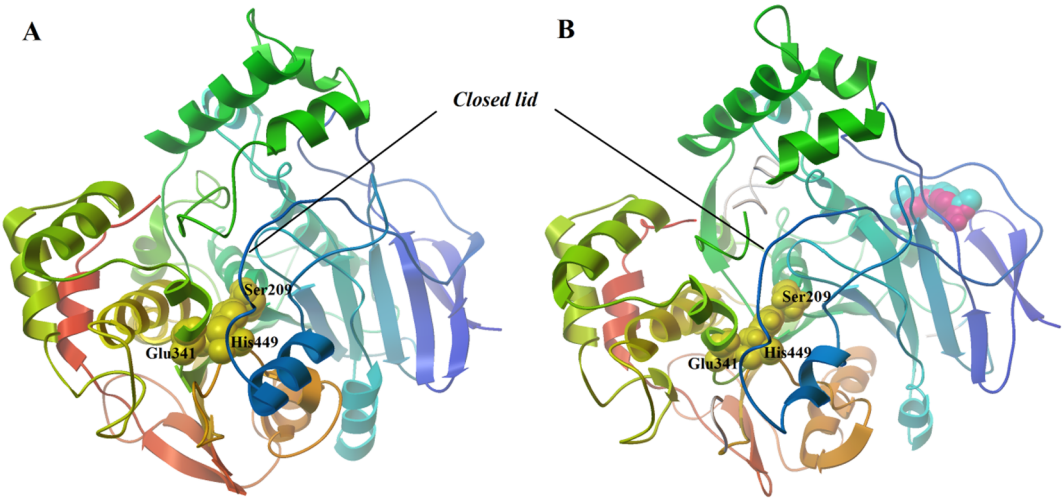

Fig. 8. A comparative view of the lid from CRL crystal structure PDB (A) and lid from CRL structure after dynamic simulation at pH 8.0 (B) LQM11 (magenta) and LQM16 (cyan) compounds are showed in the complex in the allosteric site.

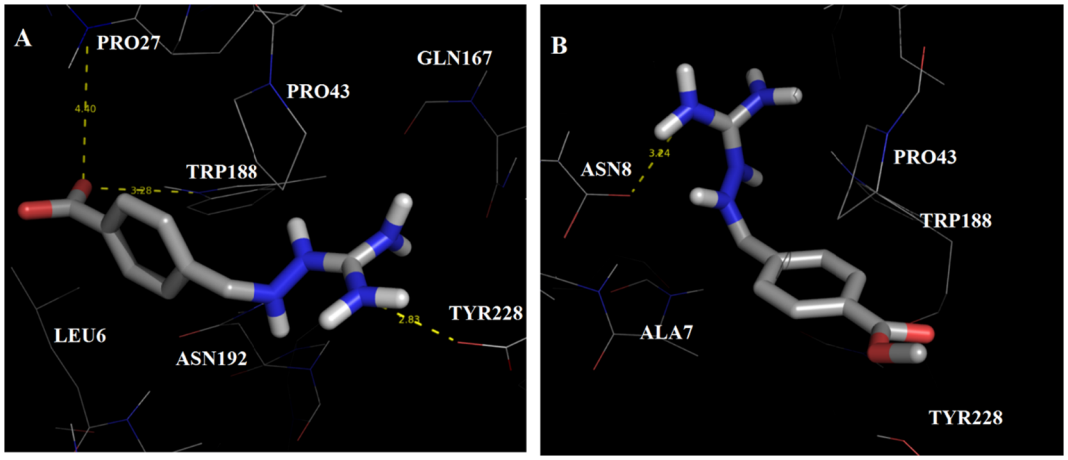

Fig. 9. Protein-ligand interactions for (A) LQM11 and (B) LQM16. Yellow dots represent hydrogen bond interactions.

Table 4
Gibbs free energy (ΔG) values predicted by M06/6-31G(d).

Compounds	Energy (kcal mol^{-1})			ΔG (kcal mol^{-1})
	$E_{complex}$	E_{enzyme}	E_{ligand}	
LQM11	−2638883.624	−2188148.415	−450703.3515	−31.85
LQM16	−2206953.38	−1712400.95	−494540.6069	−11.82

approximately the same number of atoms. However, **LQM16** showed to be more stable in its free form than **LQM11**. In contrast, it was observed a high difference in the $E_{complex}$ and E_{enzyme} values. Concerning to the complex formation ($E_{complex}$), it was demonstrated that the **LQM11** presents an excellent value, suggesting that this compound effectively interacts with the CRL enzyme, and this fact confirms that the H-bonds observed in molecular docking simulations significantly contribute to the stability of this compound in CRL-**LQM11** complex formation. In contrast, **LQM16** presents only one H-bond, corroborating with its low $E_{complex}$ value. Additionally, the binding site (E_{enzyme}) for **LQM11** is more stable than to **LQM16**, suggesting that larger binding sites are more stables. Finally, it is possible to suggest that these compounds should not only have a high $E_{complex}$ value, but their corresponding binding sites should have an excellent stability, thus contributing to final ΔG values.

3.4. Biotechnological application

The *Rhynchophorus palmarum* (Fig. 10A and B) is an agricultural pest of economic importance [65]. In this context, the guanylhydrazone derivatives were evaluated as lipase inhibitor against the crude extract of guts from *R. palmarum*, aiming a biotechnological potential application for the plague control.

In insect lipase, a similar inhibition profile for the guanylhydrazone derivatives was observed in both tissues tested. The lipase activity in the foregut (Fig. 10C) and hindgut (Fig. 10D) were significantly inhibited in 58 and 79%, respectively, by **LQM11**. The **LQM16**, however, does not cause significant inhibition in the foregut, causing lipase activity inhibition of only 17% in the hindgut (Fig. 10D). For the other derivatives the following percentages of inhibition in the foregut were observed: **LQM02** (31%), **LQM03** (27%), **LQM10** (33%), while in the hindgut the following percentages of inhibition were observed: **LQM2** (53%), **LQM03** (49%) and **LQM10** (57%). In addition, the inhibition profile (%) of insect lipase was compared to commercial enzyme (CRL), and **LQM11** was the most effective, in all systems (Fig. S5).

The results of the inhibition of lipase activity of crude insect gut extracts demonstrated inhibition profile similar to that observed for inhibition in purified CRL enzyme. The use of the crude extract in this evaluation mimics the biological conditions that occur in the insect *in vivo*, where the enzyme exerts its operation in complex and heterogeneous composition medium. Thus, as the same inhibition profile was

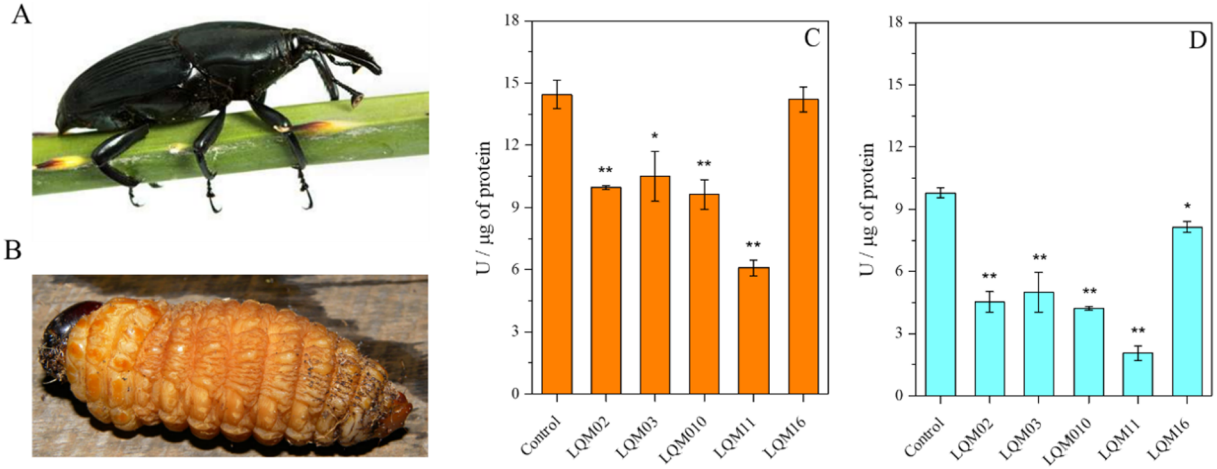

Fig. 10. *Rhynchophorus palmarum* (A) insect and (B) larvae picture. Inhibition of lipase activity of crude extract of the (C) foregut and (D) hindgut of *Rhynchophorus palmarum* larvae by the guanylhydrazone derivatives. The error bars represent the SD for the three determinations (ANOVA/Bonferroni test: $^{*}p < 0.05$; $^{**}p < 0.0001$).

observed in this condition, the inhibition of lipase activity by guanylhydrazone derivatives may be an essential and potential tool for the control of agricultural pests through interference in the insect digestion process. However, more studies will be necessary to evaluate the real potential of this biotechnological application.

4. Conclusion

The biological, biophysical and theoretical studies presented here provided evidence that **LQM11** is a potent inhibitor of lipases (CRL), when isolated or in the insect gut extracts. The guanylhydrazone derivative **LQM11** showed high affinity for the enzyme and IC_{50} lower than that of Orlistat, being a non-competitive inhibitor that binds preferentially by electrostatic interaction to an allosteric specific site of the enzyme. Thus, **LQM11** proved to be a promising compound for biotechnological application. However, further, studies are needed to evaluate the viability of this compound for this purpose.

Acknowledgments

This study was supported by grants from the Fundação de Amparo à Pesquisa do Estado de Alagoas (FAPEAL), Conselho Nacional de Desenvolvimento Científico e Tecnológico (CNPq), Financiadora de Estudos e Projetos (FINEP). This study was financed in part by the Coordenação de Aperfeiçoamento de Pessoal de Nível Superior - Brazil (CAPES) - Finance Code 001. The authors thank the students and researcher fellowships and the support of IQB-PPGQB and ESENFAR-PPGCF/UFAL. Finally, we are thankful to Maria da Graças Carvalho (UFMG) for the critical reading of the manuscript.

Appendix A. Supplementary material

Supplementary data to this article can be found online at https://doi.org/10.1016/j.bioorg.2019.03.030.

References

[1] V.R. Pinhatti, J. da Silva, T.L.C. Martins, Cytotoxic, mutagenicity, and genotoxicity effects of guanylhydrazone derivatives, Mutat. Res. 806 (2016) 1–10.
[2] N. Mayer, M. Schweiger, M.C. Melcher, C. Fledelius, R. Zechner, R. Zimmermann, R. Breinbauer, Structure-activity studies in the development of a hydrazone based inhibitor of adipose-triglyceride lipase (ATGL), Bioorg. Med. Chem. 23 (2015) 2904–2916.
[3] J. Lazić, V. Ajdačić, S. Vojnovic, M. Zlatović, M. Pekmezovic, S. Mogavero, I. Opsenica, J. Nikodinovic-Runic, Bis-guanylhydrazones as efficient anti-Candida compounds through DNA interaction, Appl. Microbiol. Biotechnol. 102 (2018) 1889–1901.
[4] I. Papanastasiou, A. Tsotinis, G. Zoidis, N. Kolocouris, S.R. Prathalingam, J.M. Kelly, Design and synthesis of Trypanosoma brucei active 1-alkyloxy and 1-benzyloxyadamantano 2-guanylhydrazones, Chem. Med. Chem. 4 (2009) 1059–1062.
[5] A. Andreani, S. Burnelli, M. Granaiola, A. Leoni, A. Locatelli, R. Morigi, M. Rambaldi, L. Varoli, N. Calonghi, C. Cappadone, G. Farruggia, New antitumor imidazo[2,1-b]thiazole guanylhydrazones and analogues, J. Med. Chem. 51 (2008) 809–816.
[6] P.R. Burney, J. Pfaendtner, Structural and dynamic features of *Candida rugosa* lipase 1 in water, octane, toluene, and ionic liquids BMIM-PF6 and BMIM-NO3, J. Phys. Chem. B 117 (2013) 2662–2670.
[7] S. Ding, J. Jiang, Z. Wang, G. Zhang, J. Yin, X. Wang, S. Wang, Z. Yu, Resveratrol reduces the inflammatory response in adipose tissue and improves adipose insulin signaling in high-fat diet-fed mice, PeerJ. 6 (2018) e5173.
[8] H.M. Kim, Y.M. Kim, J.H. Huh, E.S. Lee, M.H. Kwon, B.R. Lee, H.J. Ko, C.H. Chung, α-Mangostin ameliorates hepatic steatosis and insulin resistance by inhibition C-C chemokine receptor 2, Plos One 12 (2017) e0179204.
[9] M.L. Foresti, M.L. Ferreira, Computational approach to solvent-free synthesis of ethyl oleate using *Candida rugosa* and *Candida antarctica* B lipases. I. Interfacial activation and substrate (ethanol, oleic acid) adsorption, Biomacromolecules 5 (2004) 2366–2375.
[10] K.S. Hung, S.Y. Chen, H.F. Liu, B.R. Tsai, H.W. Chen, C.Y. Huang, J.L. Liao, K.H. Sun, S.J. Tang, C-terminal region of *Candida rugosa* lipases affects enzyme activity and interfacial activation, J. Agric. Food Chem. 59 (2011) 5396–5401.
[11] C. Otero, R. Castro, J. Soria, Electron paramagnetic resonance studies of spin-labeled fatty acid binding sites in *Candida rugosa* lipases, J. Phys. Chem. B 102 (1998) 8611–8618.
[12] S.Z. Wang, B.S. Fang, Microplate bioassay for determining substrate selectivity of *Candida rugosa* lipase, J. Chem. Educ. 89 (2012) 409–411.
[13] M.S.S. Googheri, M.R. Housaindokht, H. Sabzyan, Reaction mechanism and free energy profile for acylation of *Candida antarctica* lipase B with methylcaprylate and acetylcholine: density functional theory calculations, J. Mol. Graph. Model. 54 (2014) 131–140.
[14] A.S. de Miranda, L.S.M. Miranda, R.O.M. de Souza, Lipases: valuable catalysts for dynamic kinetic resolutions, Biotechnol. Adv. 33 (2015) 372–393.
[15] L.C. Lee, Y.T. Chen, C.C. Yen, T.C.Y. Chiang, S.J. Tang, G.C. Lee, J.F. Shaw, Altering the substrate specificity of *Candida rugosa* LIP4 by engineering the substrate-binding sites, J. Agric. Food Chem. 55 (2007) 5103–5108.
[16] A. Srivastava, C.C. Akoh, S.W. Chang, G.C. Lee, J.F. Shaw, *Candida rugosa* lipase LIP1-catalyzed transesterification to produce human milk fat substitute, J. Agric. Food Chem. 54 (2006) 5175–5181.
[17] X. Li, C. Zhang, S. Li, H. Huang, Y. Hu, Improving catalytic performance of *Candida rugosa* lipase by chemical modification with polyethylene glycol functional ionic liquids, Ind. Eng. Chem. Res. 54 (2015) 8072–8079.
[18] S. Velasco-Lozano, F. López-Gallego, R. Vázquez-Duhalt, J.C. Mateos-Díaz, J.M. Guisán, E. Favela-Torres, Carrier-free immobilization of lipase from *Candida rugosa* with polyethyleneimines by carboxyl-activated cross-linking, Biomacromolecules 15 (2014) 1896–1903.
[19] C.C. Santana, J.S. do Nascimento, M.M. Costa, A.T. da Silva, C.B. Dornelas, L.A.M. Grillo, Embryonic development of *Rhynchophorus palmarum* (Coleoptera: Curculionidae): dynamics of energy source utilization, J. Insect Sci. 14 (2014) 280.
[20] C.C. Santana, L.A. Barbosa, I.D.B. Júnior, T.G.D. Nascimento, C.B. Dornelas, L.A.M. Grillo, Lipase activity in the larval midgut of *Rhynchophorus palmarum*: biochemical characterization and the effects of reducing agents, Insects 8 (2017) 100.
[21] P.H.B. França, E.F. Silva-Júnior, P.G.V. Aquino, A.E.G. Santana, J.N.S. Ferro, E. de Oliveira Barreto, C. Do Ó Pessoa, A.S. Meira, T.M. Aquino, M.S. Alexandre-Moreira, M. Schmitt, J.X. Araújo-Júnior, Preliminary *in vitro* evaluation of the anti-proliferative activity of guanylhydrazone derivatives, Acta Pharm. 66 (2016) 129–137.
[22] S.J. Choi, J.M. Hwang, S. Kim, A colorimetric microplate assay method for high throughput analysis of lipase activity, J. Biochem. Mol. Biol. 36 (2003) 417–420.
[23] P. Diaz, N. Prim, F.I. Javier Pastor, Direct fluorescence-based lipase activity assay, Biotechniques 27 (1999) 696–698.
[24] M.M. Bradford, A rapid and sensitive method for the quantitation of microgram quantities of protein utilizing the principle of protein-dye binding, Anal. Biochem. 72 (1976) 248–254.
[25] T.C.A. Lage, T.M.S. Maciel, Y.C.C. Mota, F. Sisto, J.R. Sabino, J.C.C. Santos, I.M. Figueiredo, C. Masia, A. de Fátima, S.A. Fernandes, L.V. Modolo, *In vitro* inhibition of *Helicobacter pylori* and interaction studies of lichen natural products with jack bean urease, New J. Chem. 42 (2018) 5356–5366.
[26] M.D.A. Dantas, H.A. Tenório, T.I.B. Lope, H.J.V. Pereira, A.J. Marsaioli, I.M. Figueiredo, J.C.C. Santos, Interactions of tetracyclines with ovalbumin, the main allergen protein from egg white: spectroscopic and electrophoretic studies, Int. J. Biol. Macromol. 102 (2017) 505–514.
[27] J.C.N. Santos, I.M. Silva, T.C. Braga, A. de Fátima, I.M. Figueiredo, J.C.C. Santos, Thimerosal changes protein conformation and increase the rate of fibrillation in physiological conditions: spectroscopic studies using bovine serum albumin (BSA), Int. J. Biol. Macromol. 113 (2018) 1032–1040.
[28] M.F. Sanner, Python: A programming language for software integration and development, J. Mol. Graph. Model. 17 (1999) 57–61.
[29] D.C. Bas, D.M. Rogers, J.H. Jensen, Very fast prediction and rationalization of pKa values for protein-ligand complexes, Proteins: Struct. Funct. Bioinf. 73 (2008) 765–783.
[30] M.H.M. Olsson, C.R. Sondergaard, M. Rostkowski, J.H. Jensen, PROPKA3: Consistent treatment of internal and surface residues in empirical pKa predictions, J. Chem. Theory Comput. 7 (2011) 525–537.
[31] K. Świderek, S. Martí, V. Moliner, Theoretical study of primary reaction of pseudozyma antarctica lipase b as the starting point to understand its promiscuity, ACS Catal. 4 (2014) 426–434.
[32] S.C. Lovell, I.W. Davis, W.B. Arendall, P.I.W. de Bakker, J.M. Word, M.G. Prisant, J.S. Richardson, D.C. Richardson, Structure validation by Cα geometry: φ, ψ and Cβ deviation, Proteins Struct. Funct. Genet. 50 (2003) 437–450.
[33] V.Y. Martiny, F. Martz, E. Selwa, B.I. Iorga, Blind pose prediction, scoring, and affinity ranking of the CSAR dataset, J. Chem. Inf. Model. 2015 (2014) 151001125645007.
[34] X. Du, E. Hansell, J.C. Engel, C.R. Caffrey, F.E. Cohen, J.H. McKerrow, Aryl ureas represent a new class of anti-trypanosomal agents, Chem. Biol. 7 (2000) 733–742.
[35] J. Correa-Basurto, C. Flores-Sandoval, J. Marín-Cruz, A. Rojo-Domínguez, L.M. Espinoza-Fonseca, J.G. Trujillo-Ferrara, Docking and quantum mechanic studies on cholinesterases and their inhibitors, Eur. J. Med. Chem. 42 (2007) 10–19.
[36] X. Chen, QSAR and primary docking studies of trans-stilbene (TSB) series of imaging agents for β-amyloid plaques, J. Mol. Struct. Theochem. 763 (2006) 83–89.
[37] B.D. Bursulaya, M. Totrov, R. Abagyan, C.L. Brooks, Comparative study of several algorithms for flexible ligand docking, J. Comput. Aided Mol. Des. 17 (2003) 755–763.
[38] M.D. Cummings, R.L. DesJarlais, A.C. Gibbs, V. Mohan, E.P. Jaeger, Comparison of automated docking programs as virtual screening tools, J. Med. Chem. 48 (2005) 962–976.
[39] M. Kontoyianni, G.S. Sokol, L.M. Mcclellan, Evaluation of library ranking efficacy in virtual screening, J. Comput. Chem. 26 (2005) 11–22.
[40] G.L. Warren, C.W. Andrews, A.M. Capelli, B. Clarke, J. LaLonde, M.H. Lambert, M. Lindvall, N. Nevins, S.F. Semus, S. Senger, G. Tedesco, I.D. Wall, J.M. Woolven, C.E. Peishoff, M.S. Head, A critical assessment of docking programs and scoring functions, J. Med. Chem. 49 (2006) 5912–5931.

[41] R.D. Malmstrom, S.J. Watowich, Using free energy of binding calculations to improve the accuracy of virtual screening predictions, J. Chem. Inf. Model. 51 (2011) 1648–1655.
[42] E.F. Silva-Júnior, P. França, L. Quintas-Júnior, F. Mendonça-Junior, L. Scotti, M. Scotti, T.M. Aquino, J.X. Araújo-Júnior, Dynamic simulation, docking and DFT studies applied to a set of anti-acetylcholinesterase inhibitors in the enzyme β-Secretase (BACE-1): an important therapeutic target in Alzheimer's disease, Curr. Comput. Aided. Drug Des. 13 (2017) 1–9.
[43] Spartan'14 for Windows, Macintosh and Linux - Tutorial and User's Guide, 2014.
[44] V.S. Bryantsev, M.S. Diallo, A.C.T. Van Duin, W.A. Goddard, Evaluation of B3LYP, X3LYP, and M06-class density functionals for predicting the binding energies of neutral, protonated, and deprotonated water clusters, J. Chem. Theory Comput. 5 (2009) 1016–1026.
[45] Y. Zhao, D.G. Truhlar, The M06 suite of density functionals for main group thermochemistry, thermochemical kinetics, noncovalent interactions, excited states, and transition elements: two new functionals and systematic testing of four M06-class functionals and 12 other function, Theor. Chem. Acc. 120 (2008) 215–241.
[46] E.J. Barreiro, A.E. Kümmerle, C.A.M. Fraga, The methylation effect in medicinal chemistry, Chem. Rev. 111 (2011) 5215–5246.
[47] K. Benarous, I. Bombarda, I. Iriepa, I. Moraleda, H. Gaetan, A. Linani, D. Tahri, M. Sebaa, M. Yousfi, Harmaline and hispidin from *Peganum harmala* and *Inonotus hispidus* with binding affinity to *Candida rugosa* lipase: *in silico* and *in vitro* studies, Bioorganic Chem. 62 (2015) 1–7.
[48] P. Grochulski, Y. Li, J.D. Schrag, M. Cygler, Two conformational states of *Candida rugosa lipase*, Protein Sci. 3 (1994) 82–91.
[49] R. Zhang, Y. Liu, X. Huang, M. Xu, R. Liu, W. Zong, Interaction of a digestive protease, *Candida rugosa* lipase, with three surfactants investigated by spectroscopy, molecular docking and enzyme activity assay, Sci. Total Environ. 622–623 (2018) 306–315.
[50] J.R. Albani, Principles and Applications of Fluorescence Spectroscopy, Wiley-Blackwell, Oxford, 2007, pp. 145–146.
[51] C.M. da Silva, M.M. Silva, F.S. Reis, A.L.T.G. Ruiz, J.E. Carvalho, J.C.C. Santos, I.M. Figueiredo, R.B. Alves, L.V. Modolo, A. de Fátima, Studies on free radical scavenging, cancer cell antiproliferation, and calf thymus DNA interaction of Schiff bases, J. Photochem. Photobiol. B 172 (2017) 129–138.
[52] S. Das, C.J. da Silva, M.M. Silva, M.D.A. Dantas, A. de Fátima, A.L.T.G. Ruiz, C.M. da Silva, J.E. Carvalho, J.C.C. Santos, I.M. Figueiredo, E.F. Silva-Júnior, T.M. Aquino, J.X. Araújo-Júnior, G. Brahmachari, L.V. Modolo, Highly functionalized piperidines: free radical scavenging, anticancer activity, DNA interaction and correlation with biological activity, J. Adv. Res. 9 (2018) 51–61.
[53] M.M. Silva, E.O.O. Nascimento, E.F. Silva-Júnior, J.X. Araújo-Júnior, C.C. Santana, L.A.M. Grillo, R.S. Oliveira, P.R.R. Costa, C.D. Buarque, J.C.C. Santos, I.M. Figueiredo, Interaction between bioactive compound 11a-*N*-tosyl-5-deoxipterocarpan (LQB-223) and Calf thymus DNA: spectroscopic approach, electrophoresis and theoretical studies, Int. J. Biol. Macromol. 96 (2017) 223–233.
[54] P.D. Ross, S. Subramanian, Thermodynamics of protein association reactions: forces contributing to stability, Biochemistry 20 (1981) 3096–3102.
[55] M.M. Silva, F.C. Savariz, E.F. Silva, T.M. Aquino, M.H. Sarragiotto, J.C.C. Santos, I.M. Figueiredo, Interaction of β-carbolines with DNA: Spectroscopic studies, correlation with biological activity and molecular docking, J. Braz. Chem. Soc. 27 (2016) 1558–1568.
[56] L. Zhao, S. Hu, Q. Meng, M. Xu, H. Zhang, R. Liu, The binding interaction between cadmium-based, aqueous-phase quantum dots with *Candida rugosa* lipase, J Mol Recognit. (2018) e2712.
[57] R. Zhang, L. Zhao, R. Liu, Deciphering the toxicity of bisphenol a to Candida rugosa lipase through spectrophotometric methods, Photochem. Photobiol. B 163 (2016) 40–46.
[58] J. Zhang, L. Xiao, Y. Yang, Z. Wang, G. Li, Lignin binding to pancreatic lipase and its influence on enzymatic activity, Food Chem. 149 (2014) 99–106.
[59] I.M. Kuznetsova, A.I. Sulatskaya, O.I. Povarova, K.K. Turoverov, Reevaluation of ANS binding to human and bovine serum albumins: key role of equilibrium microdialysis in ligand - receptor binding characterization, PLoS One 7 (2012) e40845.
[60] I.M. Figueiredo, A.J. Marsaioli, Screening protein-ligand interactions using ^{1}H NMR techniques for detecting the ligand, Quim. Nova 30 (2007) 1597–1605.
[61] P. Grochulski, F. Bouthillier, R.J. Kazlauskas, A.N. Serreqi, J.D. Schrag, E. Ziomek, M. Cygler, Analogues of reaction intermediates identify a unique substrate binding site in *Candida rugosa* lipase, Biochemistry 33 (1994) 3494–3500.
[62] E.F. Silva-Júnior, J.X. Araújo-Júnior, T.M. Aquino, Quantum Mechanical (QM) Calculations applied to ADMET drug prediction: a review, Curr. Drug Metab. 18 (2017) 1–16.
[63] J. Barriuso, M.E. Vaquero, A. Prieto, M.J. Martínez, Structural traits and catalytic versatility of the lipases from the *Candida rugosa*-like family: a review, Biotechnol. Adv. 34 (2016) 874–885.
[64] S.A. Krawetz, D.D. Womble, 3D Molecular Visualization with Protein Explorer, in: Introduction to Bioinforma., 1a ed., Humana Press, 2003, pp. 565–585.
[65] A.C. Viana, I.G. Ramos, E.L. Santos, A.J.S. Mascarenhas, M.S. Lima, A.E.G. Sant'Ana, J.I. Druzian, Validation of analytical method for rhynchophorol quantification and stability in inorganic matrix for the controlled release of this pheromone, Chem. Cent. J. 12 (2018) 54.